

## Phenol Removal Using Granular Dead Anaerobic Sludge Permeable Reactive Barrier in a Simulated Groundwater Pilot Plant

Ayad Abdulhamza Faisal

Assistant Professor

College of Engineering-University of Baghdad  
email: ayadabedalhamzafaisal@yahoo.com

Ziad Tark Abd Ali

Ph.D. student

College of Engineering-University of Baghdad  
email: [z.teach2000@yahoo.com](mailto:z.teach2000@yahoo.com)

### ABSTRACT

This study investigates the performance of granular dead anaerobic sludge (GDAS) bio-sorbent as permeable reactive barrier in removing phenol from a simulated contaminated shallow groundwater. Batch tests have been performed to characterize the equilibrium sorption properties of the GDAS and sandy soil in phenol-containing aqueous solutions. The results of GDAS tests proved that the best values of operating parameters, which achieve the maximum removal efficiency of phenol ( $=85\%$ ), at equilibrium contact time ( $=3$  hr), initial pH of the solution ( $=5$ ), initial phenol concentration ( $=50$  mg/l), GDAS dosage ( $=0.5$  g/100 ml), and agitation speed ( $=250$  rpm). Fourier transform infrared (FTIR) analysis proved that the carboxylic acid, aromatic, alkane, alcohol, and alkyl halides groups are responsible for the bio-sorption of phenol onto GDAS.

A 2D advection-dispersion, solved numerically by computer solutions (COMSOL Multiphysics 3.5a software which is based on the finite element method, has been used to simulate the equilibrium transport of phenol within groundwater. This model is taking into account the pollutant sorption onto the GDAS and sandy soil which is represented by Langmuir equation. Numerical and experimental results proved that the barrier plays a potential role in the restriction of the contaminant plume migration. Also, the barrier starts to saturate with contaminant as a function of the travel time. A good agreement between the predicted and experimental results was recognized with root mean squared error not exceeded the 0.055.

**Key words:** granular dead anaerobic sludge, phenol, permeable reactive barrier, transport.

### حماية المياه الجوفية من التلوث بالفينول باستخدام الكتلة البايولوجية المازة كجدار تفاعلي نفاذ

زياد طارق عبد علي  
طالب دكتوراة  
كلية الهندسة-جامعة بغداد

اياد عبد الحمزة فيصل  
استاذ مساعد  
كلية الهندسة-جامعة بغداد

### الخلاصة

تهدف الدراسة الحالية الى معرفة امكانية استخدام الحماء اللاهوائية كمادة مازة عضوية ضمن الحاجز التفاعلي النفاذ في المعالجة الموقعية للمياه الجوفية لازالة الفينول من الطبقة الملوثة ذات الأعماق الضحلة. في اختبارات الدفعة تم دراسة تأثير عدة متغيرات تشغيلية لتحديد خواص عملية الامتزاز للفينول بواسطة الحماء اللاهوائية والتربة الرملية. أن افضل قيم لهذه المتغيرات والتي تم من خلالها الحصول على اعلى كفاءة ازالة للفينول ( $=88\%$ ) هي زمن التماس ( $=3$  ساعة), الدالة الحامضية ( $=5$ ), التركيز الابتدائي ( $=50$  ملغم/لتر), كمية المادة الممتزة ( $=5$  غم/100 مليلتر), وسرعة الاهتزاز ( $=250$  دورة/دقيقة). ان التحليل باستخدام الاشعة تحت الحمراء اثبت ان مجاميع الاروماتيك, الكربوكسيل وهاليدات الالكيل والكحول هي المجاميع الفعالة المسؤولة عن عملية الامتزاز البايولوجي للفينول.

تم حل معادلة انتقال الملوث الذائب ذات البعدين بواسطة برنامج الكومسول الذي يعتمد على طريقة العناصر المحددة لمحاكاة عملية انتقال الفينول خلال المياه الجوفية, ان هذا النموذج يأخذ بنظر الاعتبار عملية امتزاز الملوث على الحماء

اللاهوائية والترتبة الرملية والتي تخضع لمعادلة لانكمير. النتائج التي تم الحصول عليها من النماذج الرياضية وكذلك النتائج المختبرية اثبتت بان الجدران التفاعلية النفاذة تلعب دورا مهما في ازالة وتقييد حركة الملوث كما وبينت ان تلك الجدران تبدا بالتشبع بالملوث مع الزمن، اخيرا لوحظ وجود توافق جيد بين النتائج العملية والحلول العددية للنماذج الرياضية حيث كان جذر متوسط مربع الخطأ لا يتجاوز 0.055 .

## 1. INTRODUCTION

The treatment and protection of groundwater and surface water are the significant problems which need to be resolved as fast as possible. Groundwater can be polluted mainly with pollutants from dumping sites, municipal landfills, petrol stations, airports, agriculture, chemical plants, etc. Contaminants from the above mentioned sources flow downward in the unsaturated zone, reach the groundwater and in the form of diluted solution flow horizontally and can pollute surface water like rivers, lakes, etc. There are more than 30 types of technologies for treating groundwater and contaminated soil. Each of them is effective in particular conditions. PRB technology is an interesting method for groundwater remediation and is used when contaminants are in the saturated zone. This novel technique of groundwater remediation is a passive one; contaminants are removed from an aquifer by the flow through a reactive barrier filled with a reactive material, **Mieles, and Zhan, 2012**. The advantages of this technology include treatment of contaminants in the subsurface, complete plume capture, a passive (low energy) treatment approach that has considerably lower operation and maintenance costs and lower long-term performance monitoring costs, **Powell, et al., 2002**.

The most common technology used historically for remediation of groundwater has been ex-situ pump-and-treat technique. This technique is difficult, costly and ineffective most of the time in removing enough contamination to restore the groundwater to drinking water standards in acceptable time frames, **Gillham, and Burris, 1992**. The primary reason for the failure of pump and treat is the inability to extract contaminants from the subsurface due to hydro-geologic factors and trapped residual contaminant mass. Accordingly, PRBs technology was alternative method used to remediate groundwater contaminated with different types of contaminants. Many studies on PRBs using different types of reactive medium such as activated carbon, zeolite and others for treatment of inorganic and organic pollutants in groundwater have been achieved. The batch experiments showed that activated carbon is highly effective in removing of phenol, p-chlorophenol, and p-nitroaniline. Its extraordinarily high surface area and unique surface chemistry account for the difference in capacity with other carbonaceous materials like brown coal, graphite, and coke, **Ambrosini, 2004**. The adsorption and biodegradation processes used in PRB technology were selected to assess the possibility of removal of benzene and phenols from groundwater contaminated by a dumping site located in a city in Upper Silesia, Poland. Groundwater treatment parameters for granulated active carbon as a reactive material in adsorption process were measured with the Freundlich isotherm, and for a mixture of coarse sand and granulated peat in biodegradation process they were determined with the first-order kinetics equation, **Suponik, 2010**. A three series barrier system to treat high concentrations of TCE (= 500 mg/l) in synthetic groundwater was constructed. This system consisted of three reactive barriers using iron fillings as an iron-based barrier in the first column, sugarcane bagasse mixed with anaerobic sludge as an anaerobic barrier in the second column, and a biofilm coated on oxygen carbon inducer releasing material as an aerobic barrier in the third column. The efficiency of the three series barrier system in removing TCE was approximately 84% in which the removal efficiency of TCE by the iron filling barrier, anaerobic barrier and aerobic barrier were 42%, 16% and 25%, respectively, **Teerakun, et al., 2011**.

The regular biological activities of municipal wastewater treatment plants release large quantities of by-product granular dead anaerobic sludge (GDAS). Thus, re-using of this by-

product as a reactive medium in PRBs is attractive in terms of sustainable development, and reduced disposal costs. Accordingly, the aims of the present study are: (1) investigation the sorption of phenol (Ph) onto GDAS and sandy soil; (2) finding the predominant functional groups responsible of phenol removal process depended on the Fourier transfer infrared spectroscopy (FTIR) analysis; and (3) characterization the 2D equilibrium transport of Ph theoretically, using COMSOL Multiphysics 3.5a (2008) software, and compare it with experimental data.

## 2. MATERIALS AND METHODS

### 2.1 Medium and Contaminant

The GDAS was dried at atmospheric temperature for 5 days and, then, sieved into (1/0.6) mm diameter mesh. This portion was washed five times in distilled water and dried at 70°C for 6 hours prior to usage, **Mathews, and Zayas, 1989**. Table 1 shows the physical and chemical characteristics of GDAS used in the present study. These characteristics were measured in the Oil Research and Development Centre / Ministry of Oil / Iraq.

The sandy soil, with porosity of 0.41, was used as aquifer in the conducted experiments. This soil had a particle size distribution ranged from 63  $\mu\text{m}$  to 0.71 mm with an effective grain size,  $d_{10}$ , of 110  $\mu\text{m}$ , a median grain size,  $d_{50}$ , of 180  $\mu\text{m}$  and a uniformity coefficient,  $C_u = d_{60}/d_{10}$ , of 1.73. The hydraulic conductivity and bulk density equal to  $4.22 \times 10^{-3}$  cm/s and  $1.563$  g/cm<sup>3</sup>, respectively Phenol (manufactured by BDH, England) was selected as a representative of organic contaminants.

The required tests for specifying the characteristics of the soil and GDAS are carried out at; Iraqi Geological Survey-Ministry of Industry and Minerals, and Oil Research and Development Centre-Ministry of Oil.

### 2.2 Batch Experiments

These tests were carried out to specify the best conditions of contact time, initial pH of the solution, initial concentration of contaminant, dosage of sorbent and agitation speed. Six flasks of 250 ml are employed and each flask is filled with 100 ml of Ph solution which has initial concentration of 50 mg/l and initial pH=5. About 0.25 g of adsorbent was added into each flask and these flasks were kept stirred in the high-speed orbital shaker at 250 rpm. A fixed volume (20 ml) of the solution was withdrawn from each flask after different periods of time. This withdrawn solution was filtered to separate the adsorbent and a fixed volume (10 ml) of the clear solution was pipetted out for the concentration determination of phenol still present in solution. The measurements were carried out using high performance liquid chromatography (HPLC) (SHIMADZU, JAPAN). The adsorbed concentration of phenol on the reactive material was obtained by a mass balance. These tests were conducted with different values of initial pH (3, 4, 5, 6 and 7), initial concentration of Ph (50, 100, 150, 200 and 250 mg/l), adsorbent dosage (0.15, 0.25, 0.5, 1, 2 and 3 g added for 100 ml of solution) and agitation speed (0, 50, 100, 150, 200 and 250 rpm). From the best experimental results, the amount of phenol retained in the GDAS phase,  $q_e$ , was calculated using Eq.(1), **Wang, et al., 2009**:

$$q_e = (C_o - C_e) \frac{V}{m} \quad (1)$$

where  $C_o$  and  $C_e$  are the initial and equilibrium concentrations of phenol in the solution (mg/l),  $V$  is the volume of solution (l), and  $m$  is the mass of GDAS (g).

### 2.3 Description of Equilibrium Isotherm Data

They were produced by plotting the  $q_e$  against the  $C_e$  at constant temperature. Six isotherm models are used for the description of sorption data as follows, **Hamdaoui, and Naffrechoux, 2007**.

- **Langmuir model:** assumes uniform energies of adsorption onto the surface and no transmigration of adsorbate in the plane of the surface. It can be written as:

$$q_e = \frac{q_m b C_e}{1 + b C_e} \quad (2)$$

$q_m$  is the maximum adsorption capacity (mg/g) and  $b$  is the constant related to the free energy of adsorption (l/mg).

- **Freundlich model:** is quantified by:

$$q_e = K_F C_e^{1/n} \quad (3)$$

where  $K_F$  is the Freundlich sorption coefficient and  $n$  is an empirical coefficient indicative of the intensity of the adsorption.

- **Elovich model:** is based on a kinetic principle assuming that the adsorption sites increase exponentially with adsorption, which implies a multilayer adsorption. It can be expressed as:

$$\frac{q_e}{q_m} = K_E C_e \exp\left(-\frac{q_e}{q_m}\right) \quad (4)$$

where  $K_E$  is the Elovich equilibrium constant (l/mg) and  $q_m$  is the Elovich maximum adsorption capacity (mg/g).

- **Temkin model:** assumes that the heat of adsorption of all the molecules in the layer decreases linearly with coverage due to adsorbent–adsorbate interactions, and that the adsorption is characterized by a uniform distribution of the binding energies, up to some maximum binding energy. This model is given by:

$$\theta = \frac{RT}{\Delta Q} \ln K_o C_e \quad (5)$$

where  $\theta (=q_e/q_m)$  is the fractional coverage,  $R$  is the universal gas constant ( $\text{kJ mol}^{-1} \text{K}^{-1}$ ),  $T$  is the temperature (K),  $\Delta Q$  is the variation of adsorption energy ( $\text{kJ mol}^{-1}$ ), and  $K_o$  is the Temkin equilibrium constant (l/mg).

- **Kiselev model:** is known as the adsorption isotherm in localized monomolecular layer and can be expressed by:

$$k_1 C_e = \frac{\theta}{(1-\theta)(1+k_n \theta)} \quad (6)$$

where  $k_1$  is the Kiselev equilibrium constant (l/mg),  $\theta (=q_e/q_m)$  is the fractional coverage, and  $k_n$  is the constant of complex formation between adsorbed molecules.

- **Hill–de Boer model:** describes the case where there are mobile adsorption and lateral interaction among adsorbed molecules. This model is given by:

$$k_1 C_e = \frac{\theta}{1-\theta} \exp\left(\frac{\theta}{1-\theta} - \frac{k_2 \theta}{RT}\right) \quad (7)$$

where  $k_1$  is the Hill–de Boer constant (l/mg), and  $k_2$  is the energetic constant of the interaction between adsorbed molecules (kJ/mol).

## 2.4 Continuous Experiments

**Fig.1** shows the schematic diagram of the bench-scale model aquifer used in the present study. The simulated Ph transport was performed in a two-dimensional tank. The bench-scale model aquifer is contained within a rectangular 6 mm thick Perspex glass tank (100 cm L × 40 cm W × 10 cm D). This means that all sides of the tank were transparent to allow for visual observations. Two vertical perforated plates as partitions covered with filtration screen were used. These partitions are provided the lateral boundaries of the sand-filled middle compartment which has dimensions 80×40×10 cm. The purpose of the two outer compartments, i.e. influent and effluent chambers, was controlling the position of the watertable within the model aquifer deposited in the middle compartment and, in addition, controlling the wetting of this aquifer mass. Each outer compartment has dimensions of 10 cm long, 40 cm width and 10 cm high. The flow through the model aquifer was accomplished by storage tank, two constant head tanks, and flow-meter. One value of flow rate (1000 ml/min) is selected here with corresponding seepage velocity equal to 175.6 m/day.

Sampling plate, **Fig.2**, was placed on the top of the Perspex glass tank to support the sampling ports. This plate contains 4 columns and 2 rows of sampling ports designated from P1 to P8. Aqueous samples from the model aquifer were collected using stainless syringes at specified periods. The contaminant solution was introduced through the model aquifer from cubic source which was located at side of the aquifer. This source (5 cm D x 10 cm W x 10 cm L) was simulated a continuous release of contamination.

At the beginning of each test, the middle compartment was packed with 5 cm depth model aquifer. The model aquifer consisted from three parts. The first part represented by 60 cm long of the sandy soil measured from left side of the tank. The second part represented by 10 cm long barrier of reactive material placed beside the packed soil. Again, 10 cm of the sandy soil represented the third part was placed beside this barrier. The aquifer was then filled with water and left overnight to settle and saturate of this soil. Then, the packed aquifer was flushed at maximum velocity until the effluent water was free of suspended fine material.

Monitoring of Ph concentrations within the aquifer model in the effluent from sampling ports was conducted for a period of 5 day. Water sample of (3-5) ml volume was taken regularly (after 0.5, 1, 2, 3, 4 and 5 day) from each port. The samples were immediately introduced in glass vials and then analyzed by HPLC. At the end of each experiment, the soil was removed from the tank. The tank was soaked in a dilute NaOH solution and then rinsed first with tap water and finally with distilled water to avoid cross contamination between experiments.

A tracer experiment, adopted the same procedure of, **Ujfaludi, 1986**, was performed to determine the effective longitudinal dispersion coefficient for the sandy soil and GDAS.

## 2.5 FTIR Analysis of GDAS

This analysis has been considered as a kind of direct means for investigating the sorption mechanisms by identifying the functional groups responsible for binding of Ph onto GDAS, **Chen, et al., 2008**. The characteristics bands of the GDAS before and after the Ph uptake at pH= 5 were used to assess the changes in the functional groups of this material. Flask of 250 ml was filled with 100 ml of contaminant solution with concentration of 50 mg/l and 0.5 g of GDAS was

added. The flask was agitated for equilibrium time at 250 rpm. Infrared spectra of GDAS samples before and after bio-sorption of  $Pb^{+2}$  and Ph were examined using (SHIMADZU FTIR, 800 series spectrophotometer).

### 3. RESULTS AND DISCUSSIONS

#### 3.1 Fourier Transform Infrared (FTIR) Analysis

Infrared spectra of GDAS samples before and after bio-sorption of Ph were examined. These spectra were measured within the range  $400-4000\text{ cm}^{-1}$  as shown in **Fig. 3** and **Table 2**. The shifts in the IR frequencies support that aromatic, phosphines, carboxylic acid, alkyl halides, and alcohol groups are responsible for the bio-sorption of phenol onto GDAS, **Doke, et al., 2012**.

#### 3.2 Influence of Batch Operating Parameters

**Fig. 4** shows the effect of contact time and initial pH of solution on phenol sorption using 0.25 g of GDAS added to 100 ml of Ph solution for batch tests at 25 °C. This figure shows that the sorption rate was very fast initially and it's increased with increasing of contact time until reached the equilibrium time ( $\approx 3$  hr). This may be due to the presence of large number of adsorbent sites available for the adsorption of Ph. As the remaining vacant surfaces decreasing, the sorption rate slowed down due to formation of repulsive forces between the Ph on the solid surfaces and in the liquid phase, **El-Sayed et al., 2010**. Also, the increase in the Ph removal as the pH increases can be explained on the basis of a decrease in competition between proton and phenol for the surface sites which results in a lower columbic repulsion of the sorbing phenol. However, further increase in pH values would cause a decreasing in removal efficiency. It is clear from this figure that the maximum removal efficiency of Ph was achieved at initial pH of 5.

**Fig. 5** presents the removal efficiency of Ph as a function of different doses of GDAS ranged from 0.15 to 3 g added to 100 ml of solution. It can be observed that removal efficiency of the GDAS improved with increasing adsorbent dosage from 0.15 g to 0.5 g for a fixed phenol initial concentration.

**Fig. 6** explains that the removal efficiency of Ph decreased from 85% to 44% with increasing the initial concentration from 50 to 250 mg/l. This plateau represents saturation of the active sites available on the GDAS samples for interaction with ions of contaminant.

**Fig. 7** shows that about 8% of the phenol was removed before shaking (agitation speed= zero) and the uptake increases with the increase of shaking rate. There was gradual increase in contaminant uptake when agitation speed was increased from zero to 250 rpm at which about 85% of Ph has been removed. This can be attributed to improving the diffusion of ions towards the surface of the reactive media and, consequently, proper contact between ions in solution and the binding sites can be achieved.

#### 3.3 Sorption Isotherms

The sorption data for phenol on GDAS are fitted with linearized forms of (Langmuir, Freundlich, Temkin, Elovich, Kiselev, and Hill-de Boer) models. Additionally, the sorption data of sandy soil are fitted only with Langmuir and Freundlich models. **Table 3** presents the fitted parameters and coefficient of determination ( $R^2$ ) for each model. It is clear that the Langmuir isotherm model provided the best correlation in compared with other models. Accordingly, this model will be used to describe the sorption of Ph in the partial differential equation (PDE) governed the transport of a solute in the continuous mode.

### 3.4 Longitudinal Dispersion Coefficient

Results of the experimental runs concerned the measurement of longitudinal dispersion coefficient ( $D_L$ ) at different values of velocity ( $V$ ) for soil and GDAS are taken a linear relationship as follows:

$$D_L = 22.900 V + 0.871 \quad R^2=0.9172 \quad [\text{Soil}] \quad (8)$$

$$D_L = 53.944 V + 0.297 \quad R^2=0.9792 \quad [\text{GDAS}] \quad (9)$$

These equations are taken the general form of longitudinal hydrodynamic dispersion coefficient as follows:

$$D_L = \alpha_L V + D^* \quad (10)$$

where  $D^*$  is the effective molecular diffusion coefficient. This means that the longitudinal dispersivity ( $\alpha_L$ ) is equal to 22.9 cm for soil and 53.944 cm for GDAS.

### 3.5 Two-Dimensional Model Development

The contaminant migration in a porous medium is due to advection-dispersion processes; therefore, considering a two dimensional system (unidirectional fluid flow and 2D transient solute transport), the dissolved phenol mass balance equation may be written, as follows:

$$D_x \frac{\partial^2 C_{Ph}}{\partial x^2} + D_y \frac{\partial^2 C_{Ph}}{\partial y^2} - V_x \frac{\partial C_{Ph}}{\partial x} = \frac{\partial C_{Ph}}{\partial t} + \frac{\rho_b}{n} \frac{\partial q}{\partial t} \quad (11)$$

where  $C_{Ph}$  represents phenol mass concentration in water,  $q$  the phenol concentration on solid, and  $\rho_b$  the dry adsorbing material bulk density. Under isotherm conditions, the second term ( $q$ ) on the right hand side of this equation can be substituted by Langmuir model (Eq. (2)). Table 4 is summarized the model geometry, boundary value problem (i.e. governing equations, initial conditions, and boundary conditions), and solution procedure for simulated 2D problem adopted in the present study.

**Fig. 8** describes the predicted surface and contour plot of phenol normalized concentrations across the laboratory 2D sandy soil packed tank in the presence of PRB after 1, 3, 7, and 10 day for flow rate equal to 500 ml/min. It is clear that the propagation of contaminated plume is restricted by the GDAS in the barrier region and the functionality of barrier will decrease with time because the decreasing of retardation factor.

**Fig. 9** explains the effect of the applied flow rate, i.e. velocity of flow, on the extent and concentration magnitudes of the phenol plume. It is clear that the extent of contaminant plume in the longitudinal (X) direction is greater than transverse (Y) direction and this is consistent with assumption of unidirectional velocity adopted here. Also, highest concentrations occur in the sand bed which up-gradient of PRB. It is clear that the functionality of barrier will decrease with increasing the velocity of flow because the increasing penetration of the contaminant plume.

**Figs. 10** and **11** present the comparison between the predicted and experimental results at nodes corresponding to monitoring ports (P1 to P8) during the migration of the phenol plume at different periods of time for flow rate equal to 1000 ml/min. Concentration values in the ports (P1, P2, P3, and P4) located along the centerline of the source area ( $Y=20$  cm) are greater than that in the ports (P5, P6, P7, and P8) deviated from the centerline by 10 cm (i.e.  $Y=10$  cm). Also, one can be recognized the potential functionality of the GDAS in the retardation of the



contaminant migration when compared between the concentrations of ports (P3 and P4) or (P7 and P8). The shape of these curves is taken the S-curve in the ports located at furthest distance from line source such as P3 and P4. A good agreement between the predicted and experimental results can be observed with root mean squared error (RMSE), **Anderson, and Woessner, 1992**, not exceeded the 0.055.

#### 4. CONCLUSION

- Depended on batch tests, the best values of parameters affected on the bio-sorption/sorption process onto GDAS and sandy soil respectively were contact time=3 hr, initial pH of the solution=5, initial concentration=50 mg/l, sorbent dosage= 0.5 g/100 ml, and agitation speed=250 rpm.
- Phenol sorption data on the GDAS and soil were correlated reasonably well by the Langmuir sorption isotherm with coefficient of determination ( $R^2$ ) equal to 0.9944 and 0.9927, respectively.
- As proved by FTIR analysis, the carboxylic acid, aromatic, alkane, alcohol, and alkyl halides groups are responsible for the bio-sorption of phenol onto GDAS.
- The results of 2D numerical model under equilibrium condition proved that the GDAS barrier is efficient in the restriction of contaminant plume and the functionality of the barrier will decrease with increasing the travel time and the velocity of flow. A good agreement between the predicted and experimental results was recognized with RMSE not exceeded the 0.055.

#### REFERENCES

- Ambrosini, G. S. D., 2004, *Reactive Materials for Subsurface Remediation through Permeable Reactive Barriers*, Ph.D. Thesis, Swiss Federal Institute of Technology Zurich.
- Anderson, M. P., and Woessner, W. W., 1992, *Applied Groundwater Modeling: Simulation of Flow and Advective Transport*, 2<sup>nd</sup> Edition, Academic Press.
- Chen, J. P., Wang, L., and Zou, S. W., 2008, *Determination of Lead Bio-Sorption Properties by Experimental and Modeling Simulation Study*, Chem. Eng. J., Vol. 131, PP. 209-215.
- Doke, K. M., Yusufi, M., Joseph, R. D., and Khan, E. M., 2012, *Bio-Sorption of Hexavalent Chromium onto Wood Apple Shell: Equilibrium, Kinetic and Thermodynamic Studies*, Desalination and Water Treatment, Vol. 50, PP. 170-197.
- El-Sayed, G. O., Dessouki, H. A., and Ibrahim, S. S., 2010, *Bio-sorption of Ni(II) and Cd(II) Ions from Aqueous Solutions onto Rice Straw*, Chem. Sci. J., CSJ-9.
- Gillham, R. W., and Burris, D. R., 1992, *Recent Developments in Permeable In-Situ Treatment Walls for Remediation of Contaminated Groundwater*, Proc. Subsurface Restoration Conference, Dallas, Texas. June 21-24.
- Hamdaouia, O., and Naffrechoux, E., 2007, *Modeling of Adsorption Isotherms of Phenol and Chlorophenols onto Granular Activated Carbon Part I. Two-Parameter Models and*





*Equations Allowing Determination of Thermodynamic Parameters*, Journal of Hazardous Materials, Vol. 147, PP. 381–394.

- Mathews, A., and Zayas, I., 1989, *Particle Size and Shape Effects on Adsorption Rate Parameters*, Journal of Environ. Eng., Vol. 115, No. 1, PP. 41–55.
- Miele, J., and Zhan, H., 2012, *Analytical Solutions of One-Dimensional Multispecies Reactive Transport in a Permeable Reactive Barrier-Aquifer System*, Journal of Contaminant Hydrology, Vol. 134-135, PP. 54-68.
- Powell, W. W., Kenneth, W., Koput, J., Bowie, I., and Laurel S. D., 2002, *The Spatial Clustering of Science and Capital: Accounting for Biotech Firm – Venture Capital Relationships*, Regional Studies, Vol. 36, No. 3, PP. 299-313.
- Suponik, T., 2010, *Adsorption and Biodegradation in PRB Technology*, Environmental Protection Eng., Vol. 36, PP. 43-57.
- Teerakun, M., Reungsang, A., Lin, C. J., and Liao, C. H., 2011, *Coupling of Zero Valent Iron and Bio-Barriers for Remediation of Trichloroethylene in Groundwater*, Journal of Environmental Sciences, Vol. 23, PP. 560–567.
- Ujfaludi, L., 1986, *Longitudinal Dispersion Tests in Non-uniform Porous Media*, Hydrological Sciences Journal - des Sciences Hydrologiques, Vol. 31, No. 4, PP. 467-474.
- Wang, S., Nan, Z., Li, Y., and Zhao, Z., 2009, *The Chemical Bonding of Copper Ions on Kaolin from Suzhou, China*, Desalination, Vol. 249, PP. 991–995.

## NOMENCLATURE

$a$ = empirical constant, l/g.

$b$ = saturation coefficient, mg/g.

$C/C_o$ = normalized concentration.

$C_e$ = equilibrium concentration, mg/l.

$C_o$ = initial concentration of metal, mg/l.

$D^*$ = effective molecular diffusion coefficient, m<sup>2</sup>/sec

$D$ = hydrodynamic dispersion coefficient, m<sup>2</sup>/sec.

$K_F$ = Freundlich sorption coefficient.

$m$ = mass of zero-valent iron in the flask, g.

$n$ = porosity.

$q_e$ = amount of solute removed from solution, mg/kg.

$R$ = retardation factor.

$t$ = travel time, sec.

$V$ = volume of solution in the flask, l.

$V_x$ = velocity of flow in the direction  $x$ , m/sec.

$\alpha_L$ = longitudinal dispersivity, cm.

$\rho_b$ = bulk density of the soil, g/cm<sup>3</sup>.

**Table 1.** Physical and chemical characteristics of GDAS.

| <b>Physical properties</b>                         | <b>GDAS</b> |
|--|-------------|
| Actual density (kg/m <sup>3</sup> )                | 1741.6      |
| Apparent density (kg/m <sup>3</sup> )              | 609.9       |
| BET surface area (m <sup>2</sup> /g)               | 94.53       |
| Bed porosity                                       | 0.45        |
| Average particle diameter (mm)                     | 0.775       |
| Pore volume (cm <sup>3</sup> /g)                   | 0.544       |
| <b>Chemical properties</b>                         | <b>GDAS</b> |
| pH   | 7.5         |
| Ash content (%)                                    | 12          |
| Cation exchange capacity (CEC, meq/100 g)          | 51.153      |
| Organic volatile solid (V.S, 10 <sup>6</sup> mg/l) | 0.135       |
| Non-volatile solid (N.V.S, 10 <sup>6</sup> mg/l)   | 0.018       |

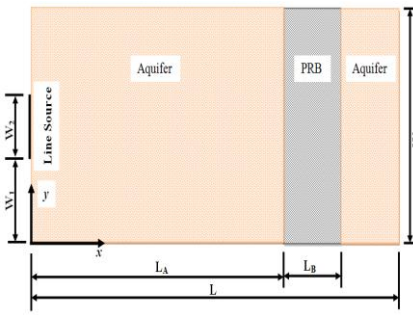
**Table 2.** Functional groups responsible for phenol bio-sorption onto GDAS.

| <b>FTIR peak</b> | <b>Wave No. (cm<sup>-1</sup>)</b> | <b>Type of bond</b>                  | <b>Functional group</b>  | <b>Displacement (cm<sup>-1</sup>)</b> |
|------------------|-----------------------------------|--------------------------------------|--------------------------|---------------------------------------|
| 1                | 514.33                            | -C-Br <sup>-</sup>                   | alkyl halides            | 4                                     |
| 2                | 796.54                            | -PH <sup>+</sup>                     | phosphines               | 11                                    |
| 3                | 875.62                            | -CH <sup>+</sup>                     | aromatic                 | 13                                    |
| 4                | 1028.11                           | -C-O-C <sup>-</sup> ,OH <sup>-</sup> | alcohol, carboxylic acid | 4                                     |
| 5                | 1086.01                           | -C-O-C <sup>-</sup>                  | alcohol                  | 2                                     |
| 6                | 1421.03                           | -OH <sup>-</sup>                     | carboxylic acid          | 3                                     |
| 7                | 1641.65                           | -CH <sup>+</sup>                     | alkane                   | 10                                    |
| 8                | 1800.99                           | -C=O <sup>-</sup>                    | carboxylic acid          | 4                                     |
| 9                | 2364.06                           | -CH <sup>+</sup>                     | alkane                   | 12                                    |
| 10               | 2519.21                           | -OH <sup>-</sup>                     | carboxylic acid          | 5                                     |
| 11               | 2855.78                           | -CH <sup>+</sup>                     | alkane                   | 10                                    |
| 12               | 2922.23                           | -CH <sup>+</sup>                     | alkane                   | 8                                     |
| 13               | 3740.11                           | -OH <sup>-</sup>                     | carboxylic acid          | 5                                     |

**Table 3.** Parameters of isotherm models for the bio-sorption of Ph onto GDAS and soil.

| Isotherm model | Parameter                                   | Phenol  |                |        |                |
|----------------|---|---------|----------------|--------|----------------|
|                |   | GDAS    | R <sup>2</sup> | Soil   | R <sup>2</sup> |
| Langmuir       | b (l/mg)                                    | 0.1410  | 0.9944         | 0.0178 | 0.9927         |
|                | q <sub>m</sub> (mg/mg)                      | 0.0252  |                | 0.0084 |                |
| Freundlich     | K <sub>F</sub> (mg/mg)(l/mg) <sup>1/n</sup> | 0.0029  | 0.9663         | 0.0007 | 0.9270         |
|                | n   | 1.4764  |                | 2.3201 |                |
| Elovich        | q <sub>m</sub> (mg/mg)                      | 0.0140  | 0.9297         | —      | —              |
|                | K <sub>E</sub> (l/mg)                       | 0.2749  |                | —      |                |
| Temkin         | ΔQ (KJ/mole)                                | 13.0124 | 0.9721         | —      | —              |
|                | K <sub>o</sub> (l/mg)                       | 1.0007  |                | —      |                |
| Kiselev        | k <sub>1</sub> (l/mg)                       | 0.1389  | 0.9942         | —      | —              |
|                | k <sub>n</sub>                              | -0.1396 |                | —      |                |
| Hill-de Boer   | k <sub>1</sub> (l/mg)                       | 0.0907  | 0.9338         | —      | —              |
|                | k <sub>2</sub> (KJ/mole)                    | 9.7621  |                | —      |                |

**Table 4.** Model geometry, boundary value problem, and solution procedure for simulated 2D problem adopted in the present study.

| Model geometry  | Governing equations  | Initial/boundary conditions (I.C./B.C.)   | Solution procedure                                |
|---|--|---|---|
|  | <p><b>Aquifer (A)</b></p> $D_{Ax} \frac{\partial^2 C_A}{\partial x^2} + D_{Ay} \frac{\partial^2 C_A}{\partial y^2} - V_{Ax} \frac{\partial C_A}{\partial x} = R_A \frac{\partial C_A}{\partial t}$ | <p><b>I.C.</b></p> $C_A(x, y, 0) = 0$ <p><b>Exterior B.C.</b></p> <ul style="list-style-type: none"> <li>• <math>C_A(0, y, t) = 0</math> except <math>C_A(0, y, t) = C_o @ W_1 \leq y \leq W_1 + W_2</math></li> <li>• <math>\frac{\partial C_A}{\partial x} = 0 @ (L, y, t)</math></li> <li>• <math>\frac{\partial C_A}{\partial y}(x, 0, t) = 0</math> and <math>\frac{\partial C_A}{\partial y}(x, W, t) = 0</math> for <math>0 \leq x \leq L_A, L_A + L_B \leq x \leq L</math></li> <li>• <math>\frac{\partial C_B}{\partial y}(x, 0, t) = 0</math> and <math>\frac{\partial C_B}{\partial y}(x, W, t) = 0</math> for <math>L_A \leq x \leq L_A + L_B</math></li> </ul>   | <p>•COMSO L Multiphysics 3.5a (2008) software</p> |
|   | <p><b>PRB (B)</b></p> $D_{Bx} \frac{\partial^2 C_B}{\partial x^2} + D_{By} \frac{\partial^2 C_B}{\partial y^2} - V_{Bx} \frac{\partial C_B}{\partial x} = R_B \frac{\partial C_B}{\partial t}$     | <p><b>I.C.</b></p> <ul style="list-style-type: none"> <li>• <math>C_B(x, y, 0) = 0</math></li> </ul> <p><b>Interior B.C.</b></p> <ul style="list-style-type: none"> <li>• <math>C_A(L_A, y, t) = C_B(L_A, y, t)</math></li> <li>• <math>C_A(L_A + L_B, y, t) = C_B(L_A + L_B, y, t)</math></li> <li>• <math>-D_{Bx} n_B \frac{\partial C_B}{\partial x} - D_{By} n_B \frac{\partial C_B}{\partial y} + V_{Bx} n_B C_B = -D_{Ax} n_A \frac{\partial C_A}{\partial x} - D_{Ay} n_A \frac{\partial C_A}{\partial y} + V_{Ax} n_A C_A @ (L_A, y, t)</math></li> <li>• <math>-D_{Bx} n_B \frac{\partial C_B}{\partial x} - D_{By} n_B \frac{\partial C_B}{\partial y} + V_{Bx} n_B C_B = -D_{Ax} n_A \frac{\partial C_A}{\partial x} - D_{Ay} n_A \frac{\partial C_A}{\partial y} + V_{Ax} n_A @ (L_A + L_B, y, t)</math></li> </ul> |   |

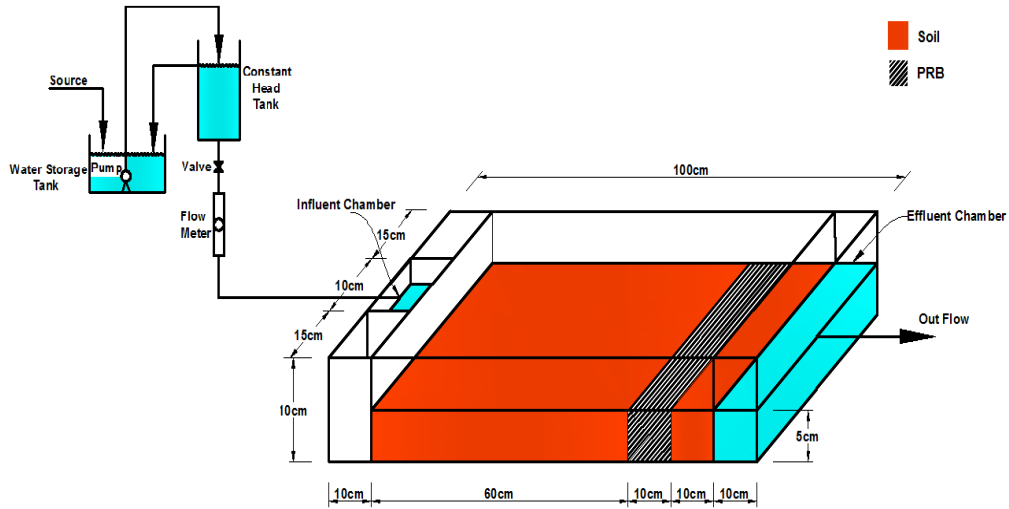


Figure 1. Schematic diagram of the bench-scale model aquifer.

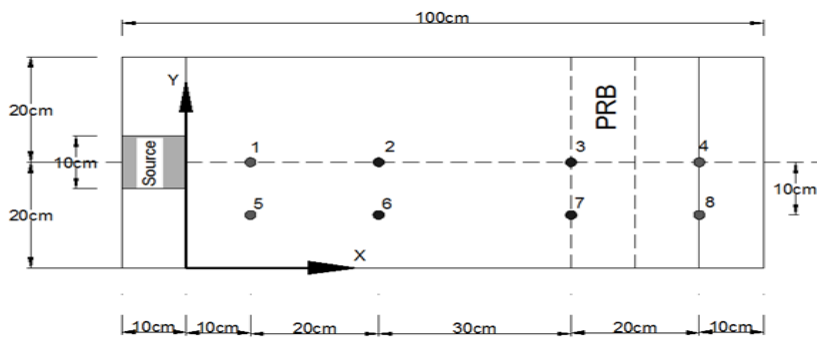


Figure 2. Schematic diagram of the sampling plate and sampling ports.

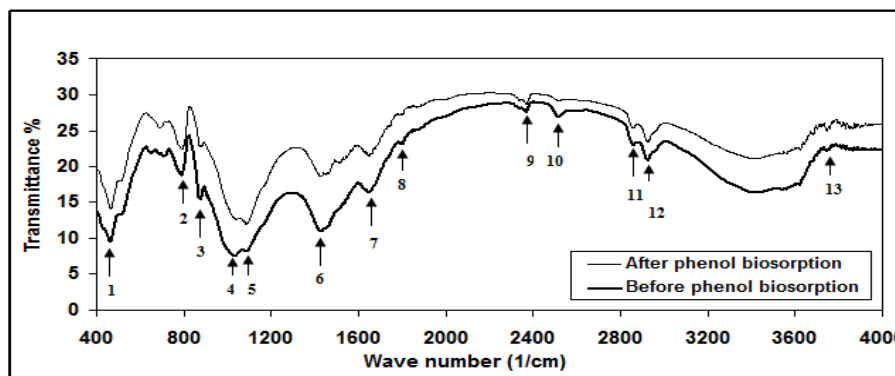
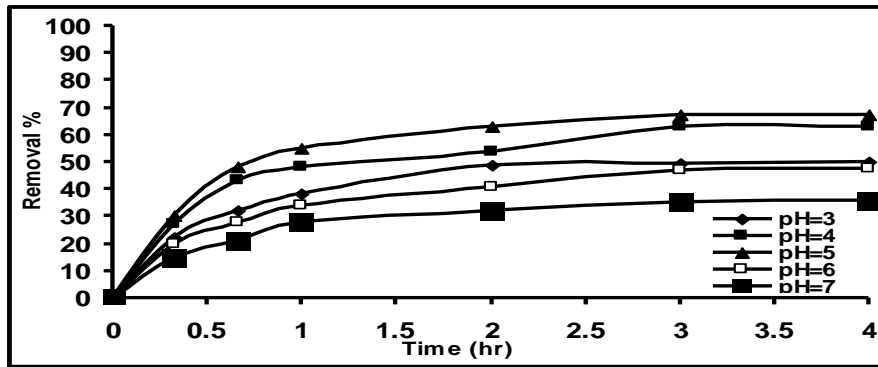
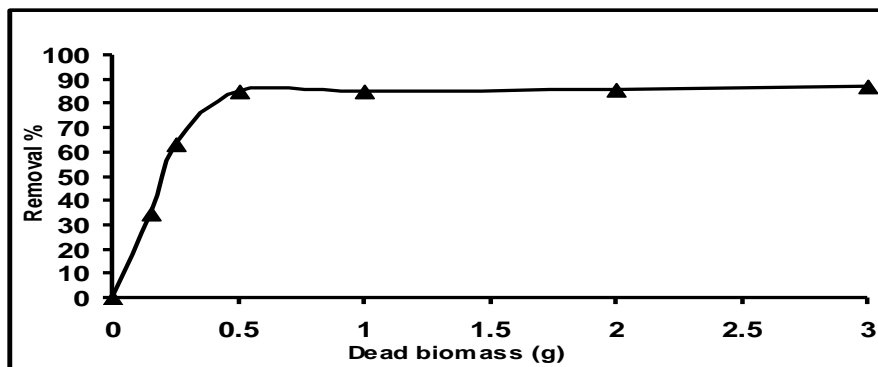


Figure 3. FTIR of GDAS before and after bio-sorption of phenol.



**Figure 4.** Removal efficiency of phenol on GDAS as a function of contact time and initial pH ( $C_0=50$  mg/l; dosage=0.25g/100 ml; agitation speed=250 rpm).



**Figure 5.** Effect of GDAS dosage on removal efficiencies of Ph ( $C_0=50$  mg/l; pH=5;  $t=3$  hr; agitation speed= 250 rpm).

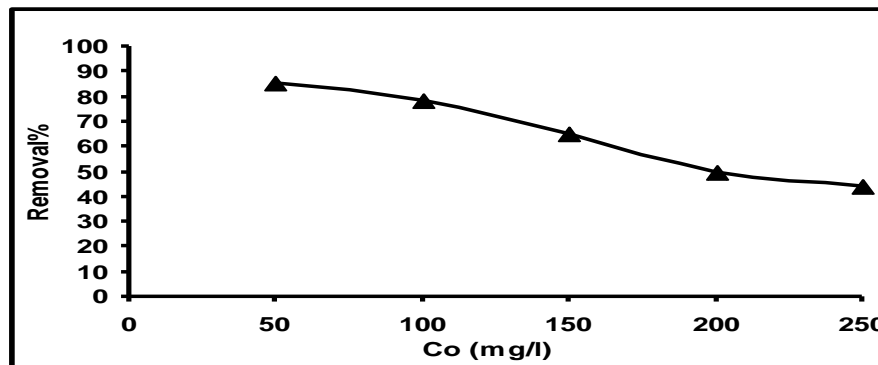


**Figure 6.** Effect of initial concentration on removal efficiency of Ph on GDAS (dosage=0.5 g/100 ml, pH=5,  $t=3$  hr, agitation speed= 250 rpm).

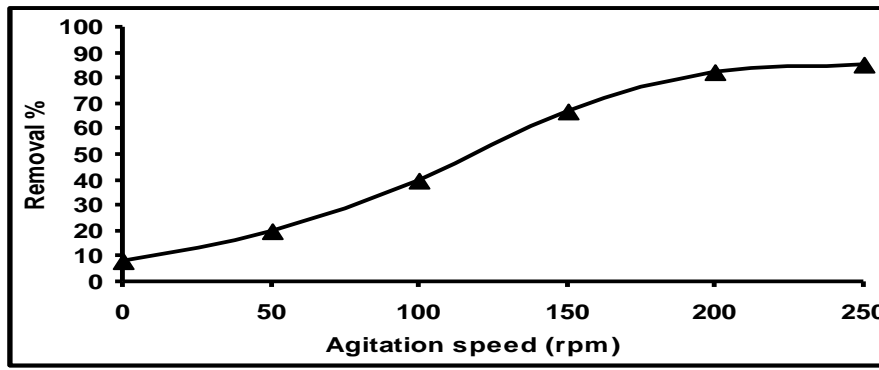
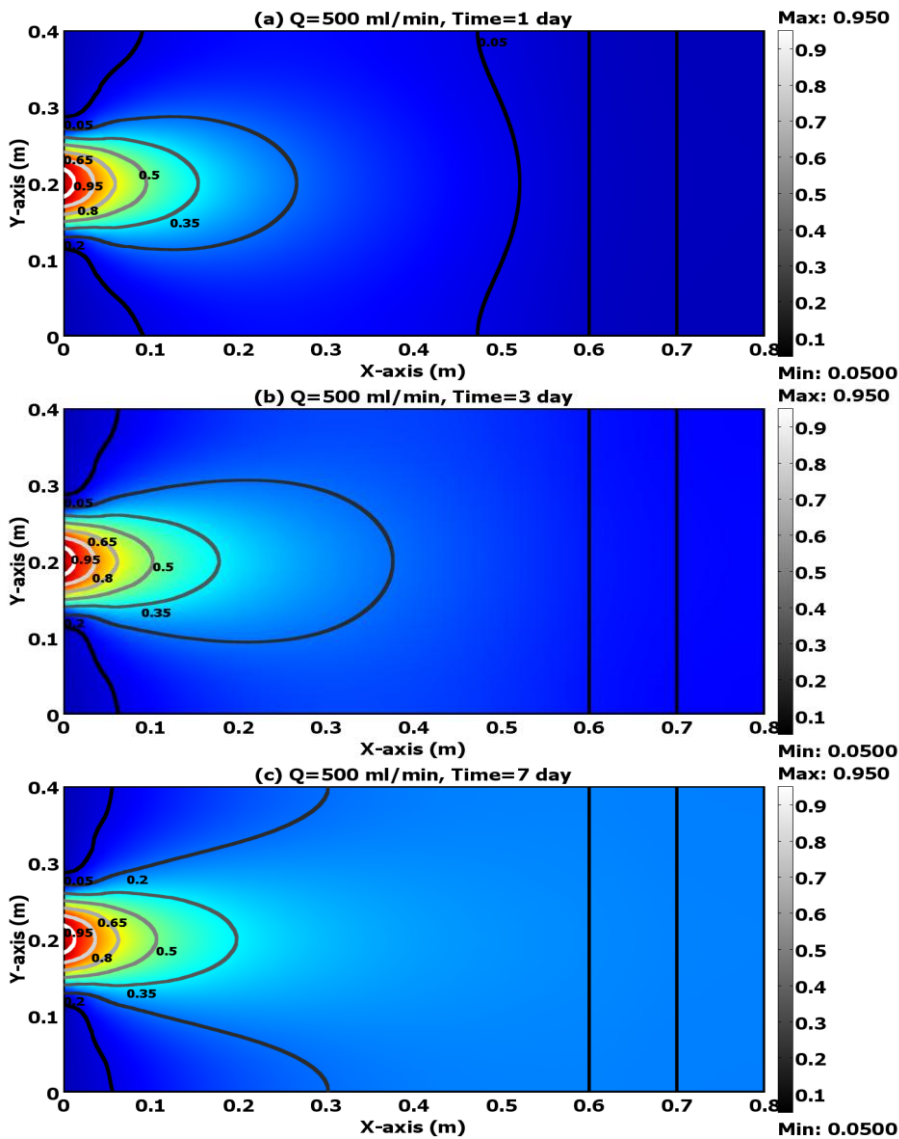
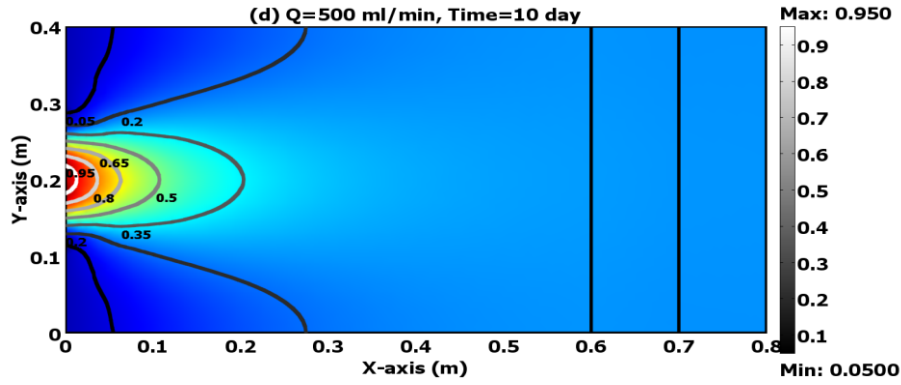
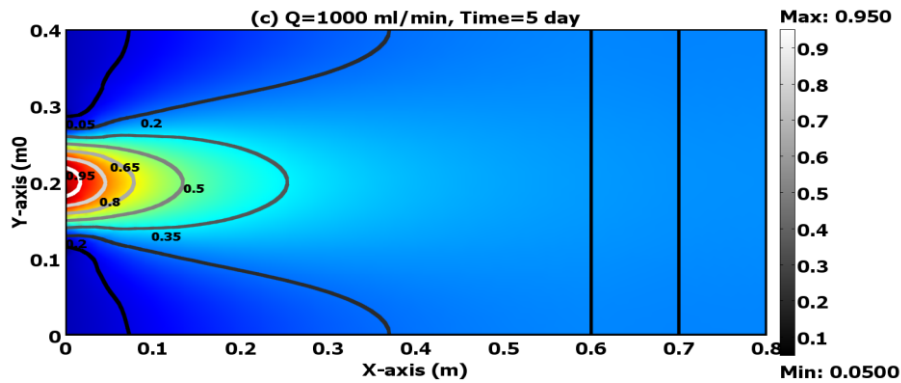
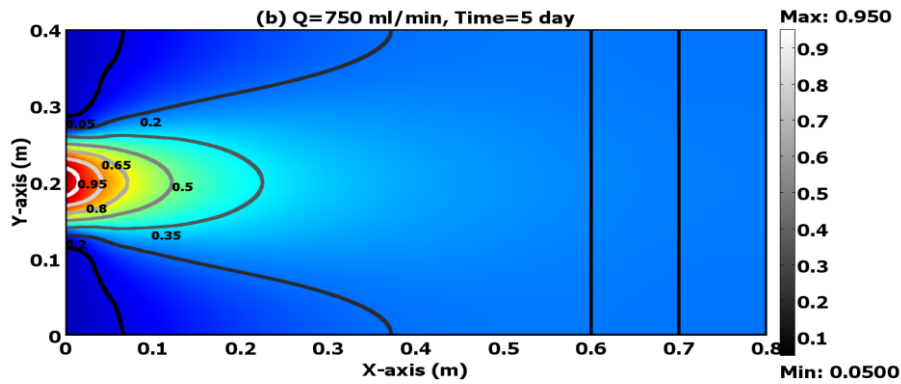
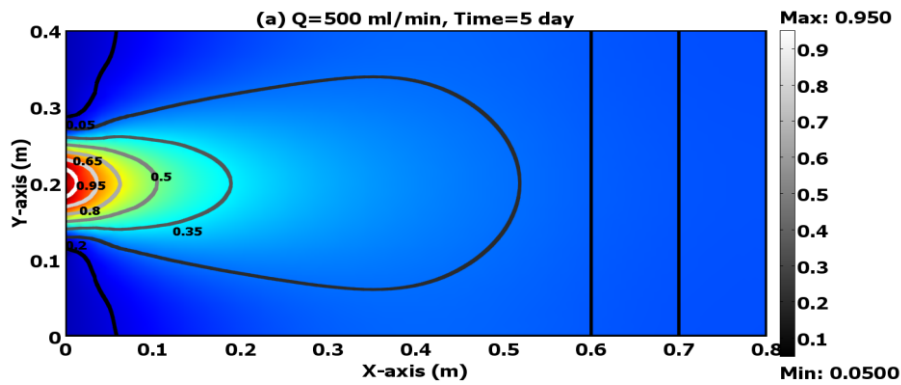


Figure 7. Effect of agitation speed on percentage removal of Ph ( $C_o=50$  mg/l, dosage=0.5 g/ 100 ml,  $t=3$  hr, pH=5).





**Figure 8.** Distribution of phenol concentration after (a) 1 (b) 3 (c) 7 and (d) 10 day for flow rate of 500 ml/min using GDAS as PRB.



**Figure 9.** Distribution of phenol concentration after 5 days for flow rate equal to (a) 500, (b) 750 and (c) 1000 ml/min using GDAS as PRB.

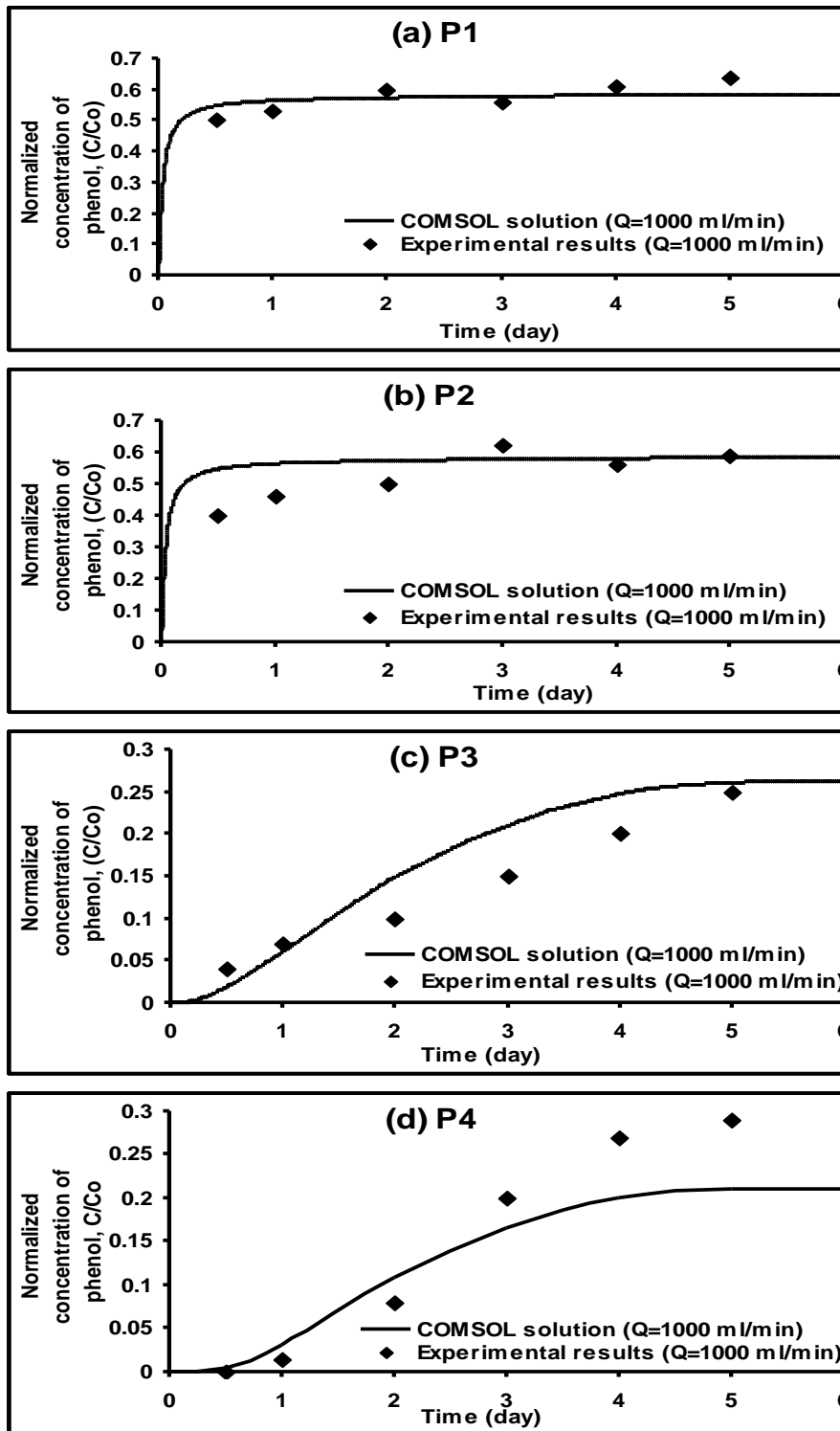
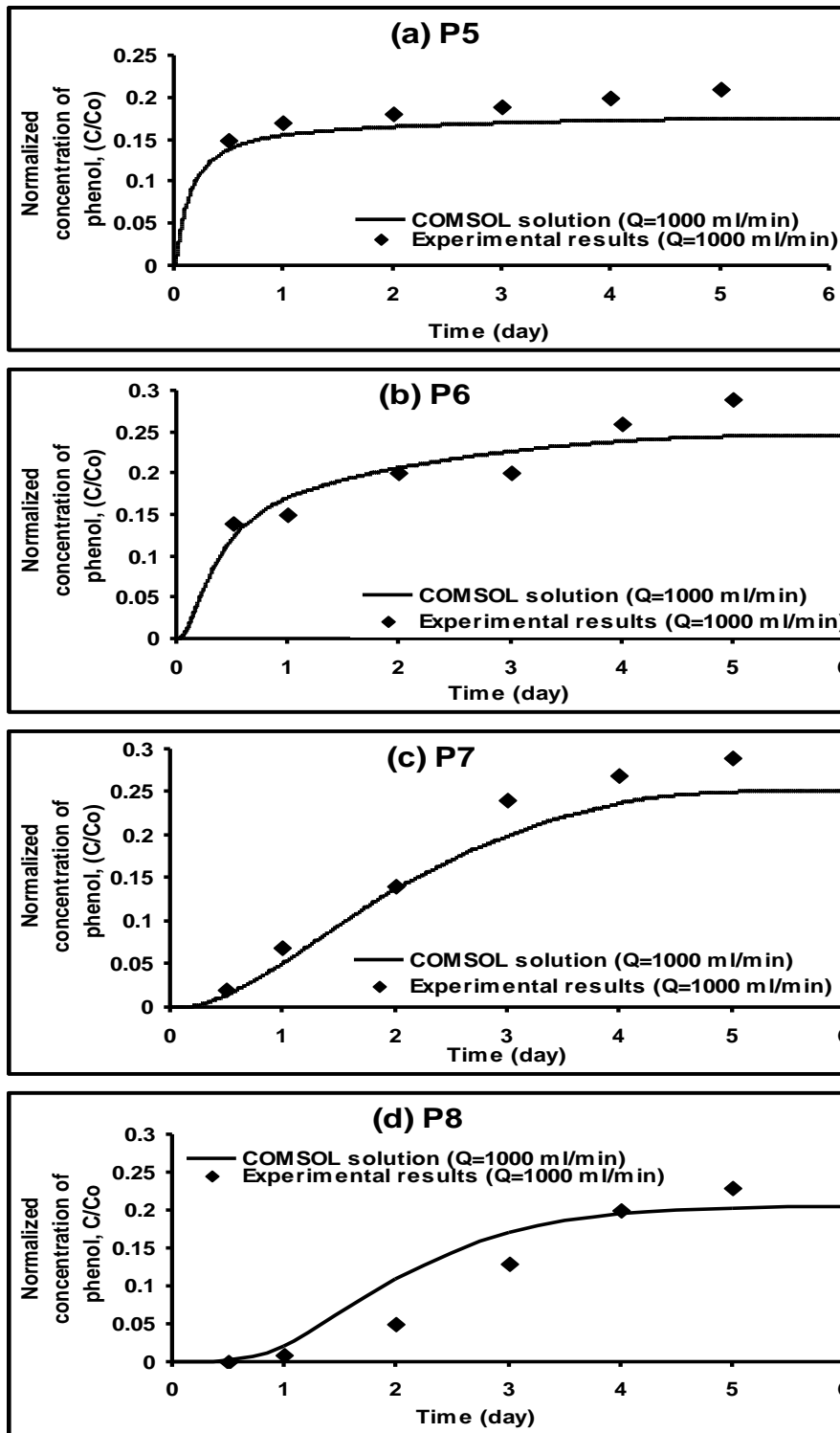


Figure 10. Breakthrough curves as a result of the phenol transport at ports (a) P1, (b) P2, (c) P3 and (d) P4 using GDAS as PRB.





**Figure 11.** Breakthrough curves as a result of the phenol transport at ports (a) P5, (b) P6, (c) P7 and (d) P8 using GDAS as PRB.